

**Shear softening and hardening of a two-dimensional Yukawa solid**Shaoyu Lu, Dong Huang, and Yan Feng <sup>\*</sup>*Center for Soft Condensed Matter Physics and Interdisciplinary Research, College of Physical Science and Technology, Soochow University, Suzhou 215006, China*

(Received 6 December 2021; accepted 23 February 2022; published 11 March 2022)

Langevin dynamical simulations are performed to study the elastic behaviors of two-dimensional (2D) solid dusty plasmas under the periodic shear deformation. The frequency- and strain-dependent shear moduli  $G(\omega, \gamma)$  of our simulated 2D Yukawa solid are calculated from the ratio of the shear stress to strain in different orientations. The shear-softening and -hardening properties in different lattice orientations are discovered from the obtained  $G(\omega, \gamma)$ . The component of the elastic constant tensor corresponding to the shear deformation is also calculated, whose variation trend exactly agrees with the discovered shear-softening and -hardening features in different shear directions. It is also found that the shear modulus of the 2D Yukawa solid always increases monotonically with the frequency.

DOI: [10.1103/PhysRevE.105.035203](https://doi.org/10.1103/PhysRevE.105.035203)**I. INTRODUCTION**

The mechanical properties of solid materials under the shear deformation are widely investigated, including many applications in materials science and engineering [1,2], such as enhancing the strength of materials [3–5]. The stress-strain response is widely used to investigate the mechanical properties for various materials or physical systems [6–17]. Typically, while undergoing a small shear deformation, the response of a solid is elastic, i.e., the stress-strain response is linear, as a result, the shear modulus can be obtained directly from the ratio of stress to strain [17]. While the applied shear deformation is large enough, i.e., in the plastic deformation regime, different mechanical behaviors can also be observed, such as shear hardening [6–10], shear softening [11–13], and shear jamming [14–16]. Here, instead of the studies above with the larger shear deformation in the plastic range [6–16], we mainly focus on the mechanical properties within the elastic range.

Dusty plasma, or complex plasma, refers to the four-component collection of highly charged micron-sized dust particles, electrons, ions, and neutral gas [18–29]. In the typical laboratory plasma conditions, the dust particles can be charged to  $\sim -10^4e$ , so that tens of thousands of dust particles can be suspended in the plasma sheath, forming a single layer, i.e., the two-dimensional (2D) dusty plasma [30,31]. Inside this 2D plane, the interaction between these dust particles can be modeled as the Yukawa repulsion of  $\phi(r) = Q^2 \exp(-r/\lambda_D)/4\pi\epsilon_0 r$ . Here,  $r$  is the distance between two particles,  $Q$  is the particle charge, and  $\lambda_D$  is the screening length. Due to their high charges, these dust particles are strongly coupled, so that their collection exhibits the collective properties of liquids [28,32–36] or solids [37–42]. While in the solid state, the 2D dusty plasma exhibits the typical elastic properties [43], and then its elastic mechanical

behaviors can be investigated at the individual particle level, as we will study here.

The elastic moduli of dusty plasmas, such as the shear modulus and the infinite frequency shear modulus [44], have been determined using different methods. In Ref. [17], the shear modulus is obtained in the elastic limit of the stress-strain relationship for 2D Yukawa solids. The approximate formula is proposed to evaluate the instantaneous shear modulus of 2D Yukawa systems in Ref. [45]. In Ref. [44], the shear modulus is determined from the potential portion of the infinite frequency shear modulus in 2D Yukawa liquids. However, from our literature search, we have not found any investigations of the elastic mechanical behaviors of solid dusty plasmas or Yukawa solids under the periodic shear deformation or their frequency-dependent shear moduli. Here, we would like to determine the frequency and strain-dependent shear moduli of solid dusty plasmas under the periodic shear deformation using computer simulations, and then investigate the elastic properties of 2D Yukawa solids.

This paper is organized as follows. In Sec. II, we introduce our Langevin dynamical simulation method to mimic the 2D solid dusty plasma under the periodic shear deformation. In Sec. III, we determine the frequency- and strain-dependent shear moduli  $G(\omega, \gamma)$  using the stress-strain response relation. From our determined  $G(\omega, \gamma)$ , we discover the shear-softening and -hardening behaviors of 2D Yukawa solids in various orientations. In addition, we also provide our interpretation of the discovered shear-softening and -hardening behaviors using the calculated elastic constants. From our literature search, we have not found any related investigations of the shear-softening and -hardening behaviors discovered in the elastic regime for any other substances at all. Finally, we briefly summarize our findings.

**II. SIMULATION METHODS**

To characterize the simulated 2D dusty plasmas, we follow the tradition [44] to use the coupling parameter  $\Gamma$  and the

<sup>\*</sup>fengyan@suda.edu.cn

screening parameter  $\kappa$ . The coupling parameter  $\Gamma$  is defined as  $\Gamma = Q^2/(4\pi\epsilon_0ak_B T)$ , where  $T$  is the kinetic temperature of dust particles,  $k_B$  is the Boltzmann constant, and  $a = (\pi n)^{-1/2}$  is the Wigner-Seitz radius for the 2D areal number density of  $n$ . The other parameter  $\kappa$  is defined as  $\kappa = a/\lambda_D$ . Here, to normalize the time and length scales, we use the nominal 2D dusty plasma frequency  $\omega_{pd} = \sqrt{Q^2/2\pi\epsilon_0ma^3}$ , and the Wigner-Seitz radius  $a$ , respectively.

We perform Langevin dynamical simulations to mimic 2D dusty plasma solids manipulated by the periodic shear deformations. The equation of motion for each particle  $i$  is [17,46,47]

$$m\ddot{\mathbf{r}}_i = -\nabla\Sigma\phi_{ij} - \nu m\dot{\mathbf{r}}_i + \zeta_i(t) + \mathbf{F}_{ex}, \quad (1)$$

where the first three terms on the right-hand side are the interparticle Yukawa repulsion, the frictional gas drag [48], and the Langevin random kicks [49], respectively. The last term of  $\mathbf{F}_{ex}$  is the external applied force of the periodic shear deformation. Our simulations are performed using LAMMPS [50], with the periodic boundary conditions in both the  $x$  and  $y$  directions.

To induce the periodic shear deformation, we apply two external forces with the same magnitude in the two opposite directions at the different locations. As shown in Fig. 1(a), each applied force is uniform within the shaded rectangular region. To study the orientation induced property variation of the 2D Yukawa solid, we choose two different shear directions, one is parallel to the lattice principal axis as in Fig. 1(b), labeled as Sim I, and the other is perpendicular to the lattice principal axis as in Fig. 1(c), labeled as Sim II. The external forces are expressed as  $F_{ex} = \pm A \cos(\omega t) ma\omega_{pd}^2$  with the oscillation frequency  $\omega$ , where  $A$  is the shear force amplitude. In our simulations, we vary the oscillation frequency  $\omega/\omega_{pd}$  from 0.005 to 0.1 to study the response of the 2D Yukawa solid, which can be easily achieved in the operation of 2D dusty plasma experiments, as Ref. [51]. For each  $\omega$ , we vary the amplitude of  $F_{ex}$ , i.e., the value of  $A$ , to obtain different shear deformations, i.e., the corresponding values of the shear strain  $\gamma$ . Note, we verify that the applied shear modulation does not produce any nonphysical effect under the periodic boundary conditions due to the low level of the shear modulation and the frictional damping in our simulated Yukawa solid.

Here are some details of our simulations. For each simulation run, we always start from a perfect crystal with  $N = 4096$  particles and specify the conditions in the solid state [52] of  $\Gamma = 800$  and  $\kappa = 0.75$ . The gas damping rate  $\nu$  is chosen as  $\nu = 0.027\omega_{pd}$ , a typical experimental value [34,36]. We set the integration time step as  $7.07 \times 10^{-3}\omega_{pd}^{-1}$  for the lower oscillation frequencies, or  $1.41 \times 10^{-3}\omega_{pd}^{-1}$  for the higher frequencies of  $\omega$ , so that the time scale is small enough to satisfy the energy conservation. When the external forces are applied, the positions and velocities of all particles are recorded in the temporal duration of  $t\omega_{pd} = 14000$  for the data analysis reported later.

The main purpose here is to investigate the mechanical behavior of the Yukawa solid under the periodic shear deformation. The data analysis is mainly focused on the relationship between the shear stress and strain of the 2D Yukawa solid. Here, we follow the tradition in the previous studies

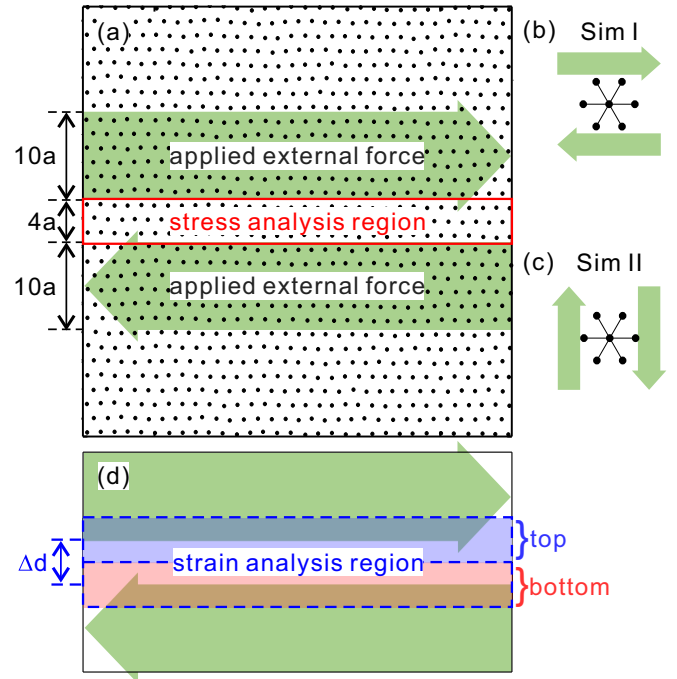


FIG. 1. Sketch of the cyclic shear modulation on two-dimensional (2D) Yukawa solids in our simulations (a). Each simulation run always starts from the perfect crystalline without defects, then the external shear manipulation  $F_{ex}/F_0 = A \cos(\omega t)$  is applied within the two shaded regions in the opposite directions. Different shear directions are specified in our simulations, labeled as Sim I for the lattice principal axis parallel to the shear direction (b), and Sim II for the lattice principal axis perpendicular to the shear direction (c). In the later data analysis, the shear stress of the central region between two shaded regions, indicated by the solid rectangular in panel (a), is calculated, while the shear strain is determined from the displacement gradient calculated from the contribution of all particles inside the dashed rectangular regions in panel (d). Note, only the central portion, i.e., 25% of the total simulation system is shown here.

with shear modulations [17,52–55] to choose the similar small analyzed region for the easier data analysis. The analyzed region of the shear stress  $\tau_{xy}$  is the central region between two external force manipulated regions, as indicated by the solid rectangular in Fig. 1(a). In our simulations, the shear stress  $\tau_{xy}$  is calculated as [17]

$$\tau_{xy} = \frac{1}{S} \sum_{i=1}^M \left[ mv_{ix}v_{iy} - \frac{1}{2} \sum_{j \neq i} \frac{x_{ij}y_{ij}}{r_{ij}} \frac{\partial \phi(r_{ij})}{\partial r_{ij}} \right], \quad (2)$$

where  $S$  and  $M$  are the area and the number of particles in the analyzed region. The particle velocities  $v_{ix}$  and  $v_{iy}$  here are just the fluctuating portions, from which the local mean flow velocity has been removed, as in Ref. [17].

The shear strain is defined as the displacement gradient along the shear direction [17], which is approximately calculated as  $\gamma = (u_{top} - u_{bottom})/\Delta d$ . Here,  $u_{top}$  and  $u_{bottom}$  are the averaged displacements over all particle within the top and bottom regions marked in Fig. 1(d). The separation between the center of the top and bottom regions is specified as  $\Delta d = 4a$ , which is just the same as the analyzed region of

the shear stress in Fig. 1(a). For the top and bottom analysis regions, we use the Cloud-in-Cell algorithm [36,56] to average the displacement along the shear direction for all particles inside, as compared with the initial lattice structure. Thus, the obtained shear strain is just the displacement gradient of the central region between two external force manipulated regions. Note, we test that the particle displacement gradient in the whole strain analysis region is almost linear for all simulations presented here, similar to Ref. [17].

Here, we would like to clarify that, we only focus on the elastic property of the 2D Yukawa solid in this paper, so that for all results presented here, there is always neither any generated defects, nor any generated nonlinear effects [57] of transverse waves due to the applied shear. Note, our simulation results are all presented in dimensionless units. Thus, the frequency, force, and stress are normalized by  $\omega_{pd}$ ,  $F_0 = ma\omega_{pd}^2$ , and  $\tau_0 = Q^2/4\pi\epsilon_0 a^3$ , respectively.

### III. RESULTS

After two manipulated forces are applied in the 2D Yukawa solid, the periodic shear deformation is generated, as one example shown in Fig. 2. The resulting shear stress  $\tau_{xy}$  exhibits a phase difference  $\pi$  with the external force  $F_{ex}$ , as shown in Fig. 2(a), from the resistance of the Yukawa solid to the external force. In Fig. 2(b), the resulting shear strain  $\gamma$  and  $F_{ex}$  oscillate simultaneously with the same phase. Thus, there is a phase difference  $\pi$  between  $\tau_{xy}$  and  $\gamma$ , and the stress-strain response relationship can be obtained by replotting the data in Figs. 2(a) and 2(b). Note, the slope of the stress-strain curve would be positive if the direction of stress is defined oppositely as in Refs. [3–5].

As shown in Fig. 2(c), we find that the stress-strain response curve almost overlap in a straight line, indicated by the dashed line there, i.e., the response of the shear stress and strain is linear. The slope of this dashed line in Fig. 2(c) is just the determined shear modulus  $G$  of our simulated system. In Fig. 2(c), the obtained shear modulus is  $G/\tau_0 = 0.037$ , agreeing with the theoretical shear modulus value  $0.034\tau_0$  obtained from the transverse sound speed of the 2D Yukawa solid [17,44]. It seems that the use of continuum descriptions in dusty plasmas is still appropriate, even for small analyzed regions in Refs. [17,51,53–55], as we do here also. Note, since only the elastic behavior of the 2D Yukawa solid is taken into account in this paper, we always specify the amplitude and frequency of the manipulated force small enough and low enough, respectively, to achieve the typical linear response of the shear stress and strain as in Fig. 2(c). The data presented in Fig. 2 comes from Sim I with the condition of  $\omega/\omega_{pd} = 0.005$  and  $F_{ex}/F_0 = 0.0014$ .

As the major result of this paper, we obtain the frequency- and strain-dependent shear moduli  $G(\omega, \gamma)$  of the 2D Yukawa solid from our simulations, as shown in Fig. 3. In Figs. 3(a) and 3(b), when the shear strain  $\gamma$  is unchanged, the shear modulus  $G$  always increases monotonically with the frequency  $\omega$ . When the frequency  $\omega$  is unchanged, for Sim I in Fig. 3(a), the shear modulus decreases monotonically with the shear strain, exhibiting a typical shear-softening feature. However, for Sim II in Fig. 3(b), when the shear strain increases, the shear modulus exhibits the reversed variation trend of increasing

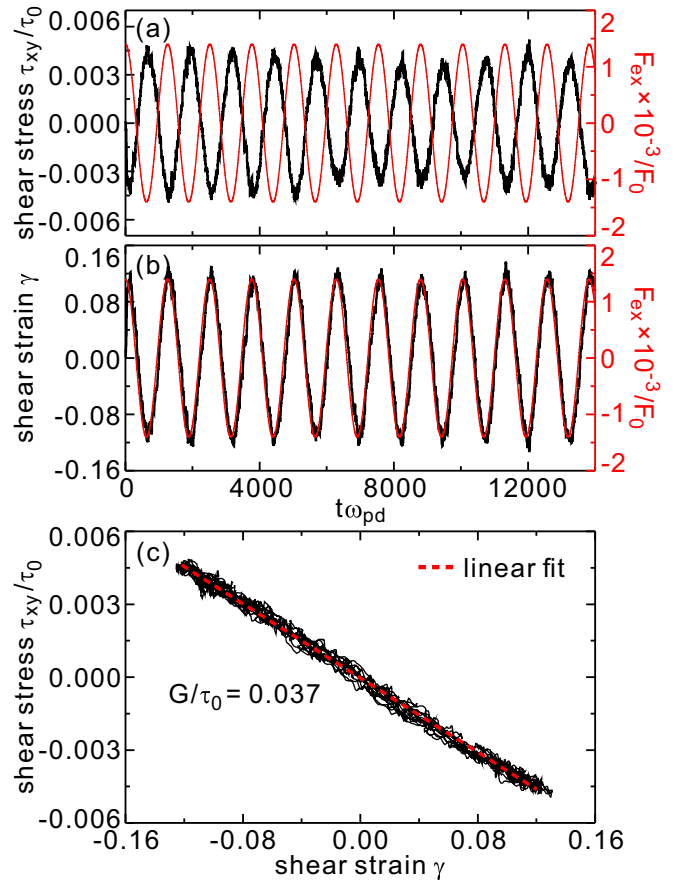


FIG. 2. Time series of the obtained shear stress  $\tau_{xy}$  (a) and shear strain  $\gamma$  (b), as well as the corresponding stress-strain response (c) from Sim I for the conditions of  $\omega/\omega_{pd} = 0.005$  and  $F_{ex}/F_0 = 0.0014$ . After applying the cyclic shear force  $F_{ex}$ , the resulting stress  $\tau_{xy}$  (a) and strain  $\gamma$  (b) both oscillate simultaneously, and there is a phase difference  $\pi$  between them. The stress-strain response curve almost overlap in a straight line, the dashed line in panel (c), suggesting that the slope of this dashed line is just the determined shear modulus  $G$  of our studied system.

monotonically with the shear strain, i.e., the so-called shear-hardening feature. These results clearly indicate that the shear modulus of the 2D Yukawa solid is strongly dependent on the orientation of the lattice. Note, when the magnitude of the shear force is large enough, a transition from the elastic to the plastic deformation, or even to the phase transition, would occur, and some nonlinear wave effects would also generate as in Ref. [57]. As a result, the relationship between  $\tau_{xy}$  and  $\gamma$  is not linear any more, and the shear modulus cannot be directly determined this way, well beyond the scope of this paper.

To clearly present the orientation dependence of our obtained shear moduli, the typical horizontal and perpendicular profiles from the cross section views of Fig. 3 are shown in Fig. 4. In Fig. 4(a), the shear modulus increases gradually with the frequency for both lattice orientations. It is reasonable because the stiffness of most materials is more remarkable at shorter time scales. Clearly, for each frequency value in Fig. 4(a), the shear modulus from Sim II is always larger than that from Sim I. This result indicates that, for the same value of  $\gamma$ , the response of the shear modulus to frequency in the

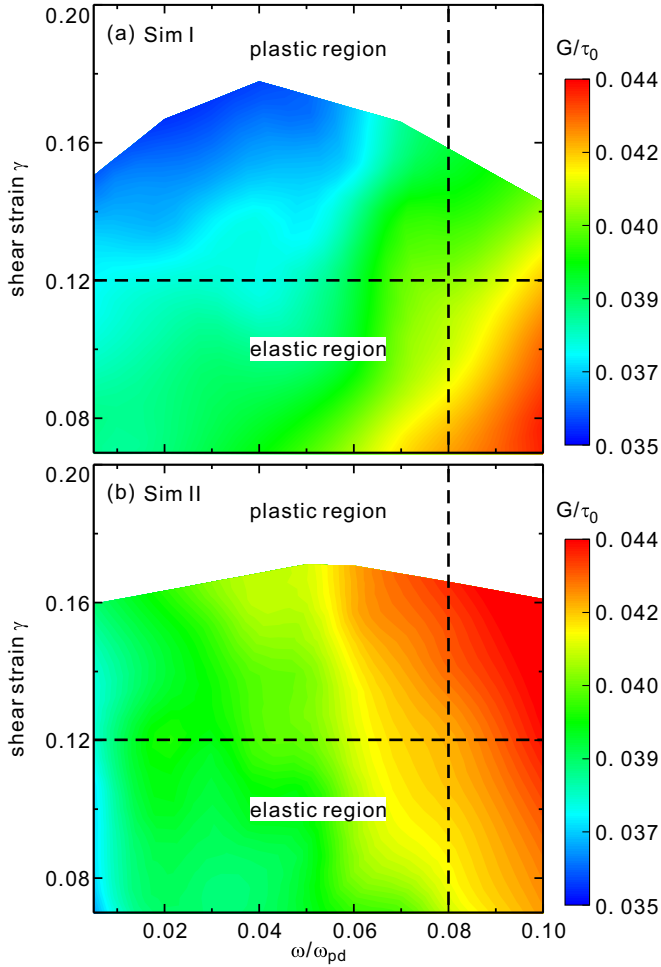


FIG. 3. Obtained frequency- and strain-dependent shear moduli  $G(\omega, \gamma)$  from Sim I (a) and Sim II (b), respectively. When the frequency  $\omega$  increases, for both Sim I and Sim II, the shear modulus increases monotonically. When the amplitude of shear strain  $\gamma$  increases, i.e., the shear strength increases, the shear modulus decreases monotonously in Sim I (a), exhibiting the shear-softening behavior. However, in Sim II (b), as the amplitude of shear strain  $\gamma$  increases, the shear modulus increases monotonously, exhibiting the reversed feature, i.e., the so-called shear-hardening behavior. Note that, for the parameters on the top of these two panels, the stress-strain response curve deviates from the linear relation of Fig. 2(c), so that the shear modulus value cannot be determined directly any more, as we will discuss at the end.

shear direction perpendicular to the lattice principal axis is more significant than that parallel to the lattice principal axis.

Our observed shear-softening and -hardening properties of 2D Yukawa solids are clearly presented in Fig. 4(b), where the shear moduli exhibit the completely opposite variation trends for the two lattice orientations, as the shear strain increases gradually. For Sim I, the shear modulus value decreases monotonically from  $0.042\tau_0$  to  $0.038\tau_0$ , reducing about 10%. However, for Sim II, the shear modulus value increases monotonically from  $0.042\tau_0$  to  $0.044\tau_0$ , increasing about 5%. In our simulations, the applied shear forces do cause the local temperature increases briefly as in Ref. [17], probably partially causing the decrease of the obtained shear modulus. The

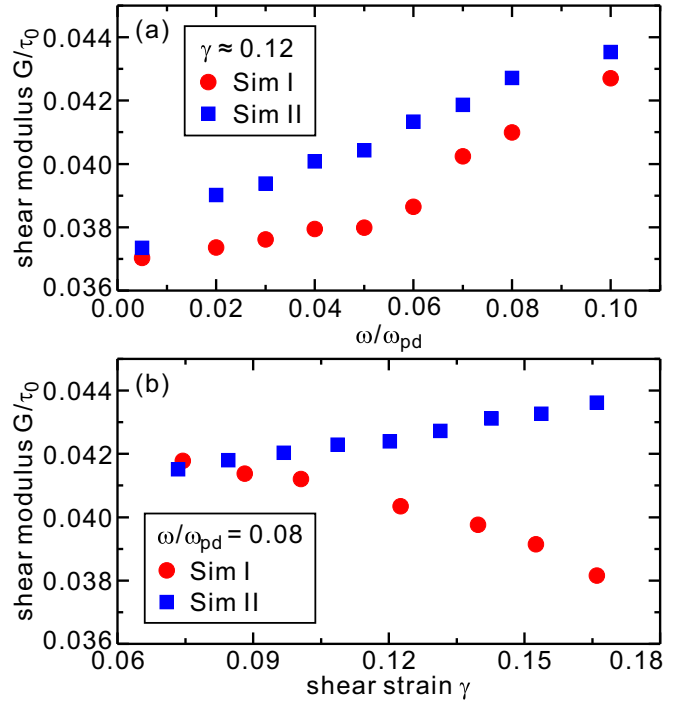


FIG. 4. Typical horizontal (a) and perpendicular (b) profiles of the obtained frequency- and strain-dependent shear moduli  $G(\omega, \gamma)$ , from the cross section views of two dashed lines in Fig. 3. In panel (a), where the shear strain is around 0.12,  $\gamma \approx 0.12$ , for both Sim I and Sim II, the shear modulus always increases monotonically with the frequency  $\omega$ . In panel (b), where the frequency is specified as  $\omega/\omega_{pd} = 0.08$ , the variation trends of the shear modulus as the function of the strain  $\gamma$  are completely different, i.e., decreasing monotonically with  $\gamma$  for Sim I, while increasing monotonically with  $\gamma$  for Sim II. Note, for the same conditions of Yukawa solids, when both the frequency and shear strength are small enough, the obtained values of the shear modulus from Sim I and Sim II are almost the same, suggesting that the effect of the lattice orientation on the shear modulus mainly happens at the shorter time scale and for the larger shear strength.

increasing temperature due to the applied shear may partially enhance the observed shear softening, however, this trend is completely reversed for the observed shear hardening. The variation range of the shear modulus value in Sim I is obviously larger than that in Sim II. These results suggest that the shear deformation along the lattice principal axis is easier than that perpendicular to the lattice principal axis.

From Figs. 4(a) and 4(b), we also find that, when the frequency  $\omega$  or shear strain  $\gamma$  is small enough, the obtained shear modulus values of two lattice orientations are almost the same. The distinctive variation trend of the shear modulus between Sim I and Sim II occurs when  $\omega$  or  $\gamma$  increases gradually. These results suggest that the effect of the lattice orientation on the shear modulus mainly happens for the larger shear strength and at the higher frequency, i.e., the shorter time scale. Note that, the simulation conditions are  $\omega/\omega_{pd} = 0.08$  and  $\gamma \approx 0.12$  for Figs. 4(a) and 4(b), respectively.

To quantitatively explain the observed shear-softening and -hardening behaviors of the 2D Yukawa solid, we use the tensor expressed stress-strain relationship, defined as  $\sigma_{ij} =$

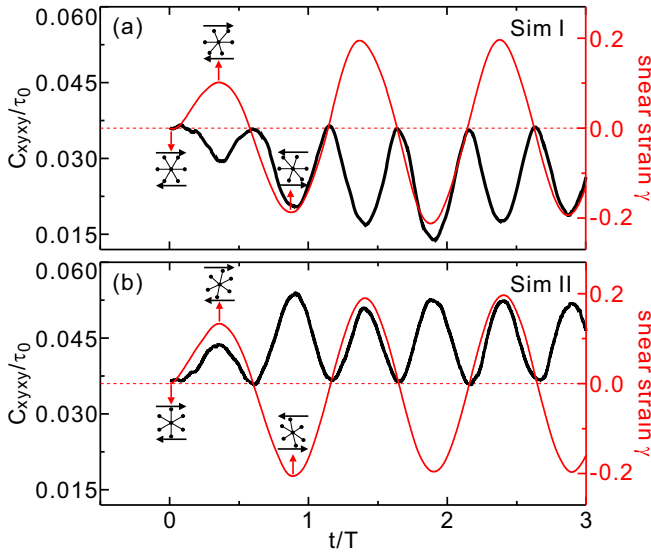


FIG. 5. Time series of the elastic constant  $C_{xyxy}$  and the resulting shear strain  $\gamma$  for Sim I (a) and Sim II (b), respectively, when two external forces are applied. For Sim I (a), in one shear deformation cycle,  $C_{xyxy}$  reaches its maximum when  $\gamma$  is zero, and then it also reaches its minimum when the absolute value of  $\gamma$  becomes its maxima. This variation clearly results in the shear-softening feature in Sim I. However, for Sim II (b), the variation trend of  $C_{xyxy}$  exactly follows the absolute value of  $\gamma$ , i.e., the completely reversed trend of (a). That is to say,  $C_{xyxy}$  in (b) reaches its minimum when  $\gamma$  is zero, and then it also reaches its maximum when the absolute value of  $\gamma$  becomes its maxima, leading to the shear-hardening feature in Sim II. Here,  $C_{xyxy}$  is calculated from the particles between two shears. Note that, the frequency  $\omega/\omega_{pd}$  of simulated data presented here are 0.08 and 0.1 for Sim I and Sim II, respectively.

$\sum_{kl} C_{ijkl} \epsilon_{kl}$ . Here,  $\sigma_{ij}$  is the  $ij$ -component of the stress tensor  $\sigma$ ,  $\epsilon_{kl}$  is the  $kl$ -component of the strain tensor  $\epsilon$ , and  $C_{ijkl}$  are the elastic constants. Based on the atomic-level theories of mechanical properties [58,59], the contribution from each particle  $i$  to the elastic constants is given by

$$C_{\alpha\beta\delta\lambda}(i) = \frac{1}{2\Omega(i)} \sum_{j \neq i} \left( \frac{\phi''(r_{ij})}{r_{ij}^2} - \frac{\phi'(r_{ij})}{r_{ij}^3} \right) [x_\alpha(j) - x_\alpha(i)] \\ \times [x_\beta(j) - x_\beta(i)][x_\delta(j) - x_\delta(i)][x_\lambda(j) - x_\lambda(i)] \\ + \frac{\phi'(r_{ij})}{r_{ij}} [x_\beta(j) - x_\beta(i)][x_\lambda(j) - x_\lambda(i)] \delta_{\alpha\delta}. \quad (3)$$

Here,  $r_{ij}$  is distance between particles  $i$  and  $j$ , the differentiations are with respect to  $r_{ij}$ ,  $\Omega(i)$  is the volume of the Wigner-Seitz cell surrounding the particle  $i$ , and  $x_\alpha(i)$  is the  $\alpha$ -component of the position vector for the particle  $i$ . For our 2D Yukawa solid simulations, the particle position vector just contains two components,  $x$  and  $y$ , so that the indices in Eq. (3) can be simplified to  $\alpha, \beta, \delta, \lambda = x, y$ . Note, the analyzed region of the elastic constants here is the same as the analyzed region of the shear stress.

To study elastic properties of the 2D Yukawa solid under the shear deformation, we just need to take the elastic constant  $C_{xyxy}$  into account, and the time series of  $C_{xyxy}$  are presented in

Fig. 5. Here, the elastic constant  $C_{xyxy}$  is calculated as  $C_{xyxy} = \frac{1}{M} \sum_{i=1}^M C_{xyxy}(i)$ . For Sim I in Fig. 5(a), the value of  $C_{xyxy}$  changes periodically and its initial value is its maximum. However, for Sim II in Fig. 5(b), the value of  $C_{xyxy}$  changes periodically and its initial value is its minimum. For both types of simulations, the initial value of  $C_{xyxy}$  is always  $0.036\tau_0$ , well agreeing with the theoretical shear modulus of the 2D Yukawa solid as in Refs. [17,44]. Note, when the shear is applied suddenly, the system has not reached the steady state, so that the amplitude of  $C_{xyxy}$  in the first period is slightly smaller in Fig. 5.

We compare the calculated elastic constant  $C_{xyxy}$  with the obtained shear strain  $\gamma$ , to explain the observed shear-softening and -hardening behaviors. As shown in Figs. 5(a) and 5(b), when  $\gamma$  is zero in each shear deformation cycle, i.e., the system is in the unsheared state,  $C_{xyxy}$  reaches its maximum for Sim I, or its minimum for Sim II. When the absolute value of  $\gamma$  becomes largest in each shear deformation, i.e., the shear deformation is largest,  $C_{xyxy}$  reaches its minimum for Sim I, or its maximum for Sim II. These two

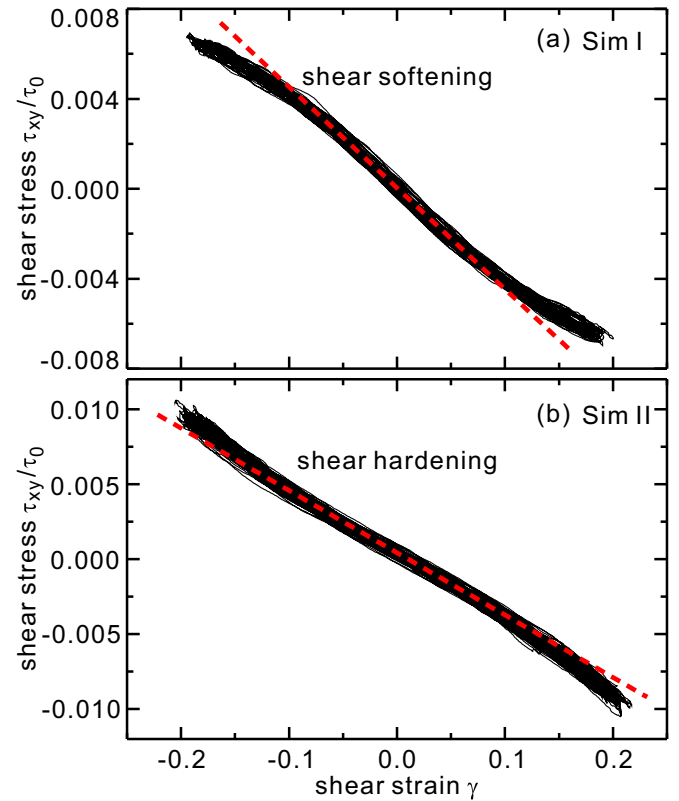


FIG. 6. Two different elastic-stress-yielding behaviors of the stress-strain responses in Sim I (a) and Sim II (b), respectively, due to the larger applied shear strength. Clearly, the stress-strain response is nearly linear in the central portion where the shear strain  $\gamma$  is smaller. However, when the shear strain  $\gamma$  is larger, the stress-strain response follows a different variation trend, i.e., a more gradual trend in Sim I (a) and a steeper trend in Sim II (b). These two different elastic-stress-yielding behaviors just correspond to the shear-softening and shear-hardening features, well consistent of our results above. Note, here the simulation conditions are  $\omega/\omega_{pd} = 0.08$  and  $0.1$  for Sim I (a) and Sim II (b), respectively.

opposite variation trends of  $C_{xyxy}$  just result in the shear-softening feature in Sim I and the shear-hardening feature in Sim II, respectively. The calculated elastic constant  $C_{xyxy}$  for each particle fluctuates over a larger range, however, the averaged  $C_{xyxy}$  results over all particles in the analysis region presented in Fig. 5 clearly exhibit the variation trends well agreeing with the discovered shear softening and hardening here, further suggesting that the shear softening and hardening are the collective properties of the Yukawa solid. Note, the simulation conditions here are  $\omega/\omega_{pd} = 0.08$  and  $0.1$  for Sim I and Sim II, respectively.

To better show the difference of the deformation with different shear directions, several typical deformation sketches of single lattice cell consisting of seven particles are also presented in Fig. 5. For each type of simulations, we choose three lattice cell sketches as representatives, corresponding to the zero, maximum, and minimum value of shear strain  $\gamma$ , respectively. Note, when the shear strain is largest, for both shear directions, the lattice deformation is still in the elastic stage, as shown in Fig. 5.

We also observed two different elastic-stress-yielding behaviors from our simulation results, as presented in Fig. 6. In Figs. 6(a) and 6(b), the central portion of the stress-strain response curve is nearly linear with the smaller shear strain  $\gamma$ . However, when the shear strain  $\gamma$  is larger, the slope of the stress-strain response changes, as the two edges shown in Figs. 6(a) and 6(b), just corresponding to the elastic-stress-yielding feature. For Sim I in Fig. 6(a), the stress-strain response curve follows a more gradual trends at both ends. However, for Sim II in Fig. 6(b), the stress-strain response curve follows a steeper trends at both ends. These different elastic-stress-yielding features also correspond to the shear-softening and shear-hardening features, well agreeing with our findings above. Further increase of the force amplitude would induce defects in the analyzed region, causing the inelastic deformation, which is beyond the scope of this paper.

Note that, when the elastic-stress-yielding behavior occurs, we do not provide the shear modulus value at those conditions any more in this paper. The simulation conditions in Fig. 6 are the same as that in Fig. 5.

#### IV. SUMMARY

In summary, we perform Langevin dynamical simulations of 2D solid dusty plasmas under the periodic shear deformation. From the obtained ratio of the shear stress to strain, we determine the frequency- and strain-dependent shear moduli  $G(\omega, \gamma)$  of the 2D Yukawa solid. We discover that the shear modulus of the 2D Yukawa solid exhibits the shear-softening and shear-hardening behaviors, when the shear is applied parallel and perpendicular to the lattice principal axis, respectively. Our discovery indicates that the shear modulus of the 2D Yukawa solid is strongly dependent on its orientation. To further verify our findings, we calculate time series of the elastic constant  $C_{xyxy}$  of these two types of simulations with different shear directions, and find that the variation trend of  $C_{xyxy}$  with the shear strain is exactly the same as the shear-softening and shear-hardening properties. Furthermore, we also observe two different elastic-stress-yielding behaviors in our simulations when the shear strength is increased further. Unlike the complicated variation trend of  $G(\omega, \gamma)$  with  $\gamma$  described above, we find that the shear modulus of 2D Yukawa solids always increases monotonically with the frequency  $\omega$  from all of our simulations.

#### ACKNOWLEDGMENTS

Work was supported by the National Natural Science Foundation of China under Grants No. 12175159 and No. 11875199, the 1000 Youth Talents Plan, startup funds from Soochow University, and the Priority Academic Program Development (PAPD) of Jiangsu Higher Education Institutions.

- 
- [1] M. A. Meyers, A. Mishra, and D. J. Benson, *Prog. Mater. Sci.* **51**, 427 (2006).
  - [2] C. Greiner, J. Gagel, and P. Gumbsch, *Adv. Mater.* **31**, 1806705 (2019).
  - [3] G. Li, S. I. Morozov, Q. Zhang, Q. An, P. Zhai, and G. J. Snyder, *Phys. Rev. Lett.* **119**, 215503 (2017).
  - [4] G. Li, U. Aydemir, S. I. Morozov, M. Wood, Q. An, P. Zhai, Q. Zhang, W. A. Goddard III, and G. J. Snyder, *Phys. Rev. Lett.* **119**, 085501 (2017).
  - [5] G. Li, Q. An, B. Duan, L. Borgsmiller, M. A. Malki, M. Agne, U. Aydemir, P. Zhai, Q. Zhang, S. I. Morozov, W. A. Goddard III, and G. J. Snyder, *Mater. Sci. Eng. R* **114**, 100607 (2021).
  - [6] K. M. Schmoller, P. Fernández, R. C. Arevalo, D. L. Blair, and A. R. Bausch, *Nat. Commun.* **1**, 134 (2010).
  - [7] P. Hiattup, A. Sirivat, and A. M. Jamieson, *J. Mater. Sci.* **45**, 1972 (2010).
  - [8] G. Liu, S. Cheng, H. Lee, H. Ma, H. Xu, T. Chang, R. P. Quirk, and S. Q. Wang, *Phys. Rev. Lett.* **111**, 068302 (2013).
  - [9] J.-C. Géminard, J. C. Pastenes, and F. Melo, *Phys. Rev. E* **97**, 042601 (2018).
  - [10] J. Pan, Y. P. Ivanov, W. Zhou, Y. Li, and A. Greer, *Nature (London)* **578**, 559 (2020).
  - [11] A. Lemaître, *Phys. Rev. Lett.* **89**, 195503 (2002).
  - [12] M. Fan, K. Zhang, J. Schroers, M. D. Shattuck, and C. S. O'Hern, *Phys. Rev. E* **96**, 032602 (2017).
  - [13] I. Lobzenko, Y. Shihara, T. Iwashita, and T. Egami, *Phys. Rev. Lett.* **124**, 085503 (2020).
  - [14] P. Urbani and F. Zamponi, *Phys. Rev. Lett.* **118**, 038001 (2017).
  - [15] R. P. Behringer and B. Chakraborty, *Rep. Prog. Phys.* **82**, 012601 (2019).
  - [16] V. Babu, D. Pan, Y. Jin, B. Chakraborty, and S. Sastry, *Soft Matter* **17**, 3121 (2021).
  - [17] B. Liu and J. Goree, *Phys. Plasmas* **24**, 103702 (2017).
  - [18] H. M. Thomas and G. E. Morfill, *Nature (London)* **379**, 806 (1996).
  - [19] L. I. W. Juan, C. Chiang, and J. Chu, *Science* **272**, 1626 (1996).
  - [20] A. Melzer, A. Homann, and A. Piel, *Phys. Rev. E* **53**, 2757 (1996).
  - [21] M. S. Murillo, *Phys. Rev. Lett.* **85**, 2514 (2000).
  - [22] R. L. Merlino and J. A. Goree, *Phys. Today* **57(7)**, 32 (2004).

- [23] G. J. Kalman, P. Hartmann, Z. Donkó, and M. Rosenberg, *Phys. Rev. Lett.* **92**, 065001 (2004).
- [24] V. E. Fortov, A. V. Ivlev, S. A. Khrapak, A. G. Khrapak, and G. E. Morfill, *Phys. Rep.* **421**, 1 (2005).
- [25] G. E. Morfill and A. V. Ivlev, *Rev. Mod. Phys.* **81**, 1353 (2009).
- [26] A. Piel, *Plasma Physics* (Springer, Heidelberg, 2010).
- [27] M. Bonitz, C. Henning, and D. Block, *Rep. Prog. Phys.* **73**, 066501 (2010).
- [28] A. Melzer, A. Schella, J. Schablinski, D. Block, and A. Piel, *Phys. Rev. E* **87**, 033107 (2013).
- [29] E. Thomas, Jr., U. Konopka, R. L. Merlino, and M. Rosenberg, *Phys. Plasmas* **23**, 055701 (2016).
- [30] Y. Feng, J. Goree, and B. Liu, *Phys. Rev. Lett.* **100**, 205007 (2008).
- [31] K. Qiao, J. Kong, J. Carmona-Reyes, L. S. Matthews, and T. W. Hyde, *Phys. Rev. E* **90**, 033109 (2014).
- [32] Z. Donkó, J. Goree, P. Hartmann, and K. Kutasi, *Phys. Rev. Lett.* **96**, 145003 (2006).
- [33] C.-L. Chan and L. I., *Phys. Rev. Lett.* **98**, 105002 (2007).
- [34] B. Liu and J. Goree, *Phys. Rev. Lett.* **100**, 055003 (2008).
- [35] T. Ott and M. Bonitz, *Phys. Rev. Lett.* **103**, 195001 (2009).
- [36] Y. Feng, J. Goree, and B. Liu, *Phys. Rev. Lett.* **104**, 165003 (2010).
- [37] M. S. Murillo, *Phys. Plasmas* **11**, 2964 (2004).
- [38] A. Melzer, A. Schella, J. Schablinski, D. Block, and A. Piel, *Phys. Rev. Lett.* **108**, 225001 (2012).
- [39] P. Hartmann, A. Douglass, J. C. Reyes, L. S. Matthews, T. W. Hyde, A. Kovács, and Z. Donkó, *Phys. Rev. Lett.* **105**, 115004 (2010).
- [40] C. Durniak and D. Samsonov, *Phys. Rev. Lett.* **106**, 175001 (2011).
- [41] P. Hartmann, A. Z. Kovács, A. M. Douglass, J. C. Reyes, L. S. Matthews, and T. W. Hyde, *Phys. Rev. Lett.* **113**, 025002 (2014).
- [42] E. Thomas, Jr., B. Lynch, U. Konopka, R. L. Merlino, and M. Rosenberg, *Phys. Plasmas* **22**, 030701 (2015).
- [43] A. Piel, V. Nosenko, and J. Goree, *Phys. Plasmas* **13**, 042104 (2006).
- [44] K. Wang, D. Huang, and Y. Feng, *Phys. Rev. E* **99**, 063206 (2019).
- [45] S. Khrapak and B. Klumov, *Phys. Plasmas* **25**, 033706 (2018).
- [46] L.-J. Hou, A. Piel, and P. K. Shukla, *Phys. Rev. Lett.* **102**, 085002 (2009).
- [47] Z. Donkó, J. Goree, and P. Hartmann, *Phys. Rev. E* **81**, 056404 (2010).
- [48] B. A. Klumov and G. E. Morfill, *JETP Lett.* **90**, 444 (2009).
- [49] Y. Feng, B. Liu, and J. Goree, *Phys. Rev. E* **78**, 026415 (2008).
- [50] See <http://lammmps.sandia.gov>.
- [51] P. Hartmann, M. C. Sándor, A. Kovács, and Z. Donkó, *Phys. Rev. E* **84**, 016404 (2011).
- [52] P. Hartmann, G. J. Kalman, Z. Donkó, and K. Kutasi, *Phys. Rev. E* **72**, 026409 (2005).
- [53] V. Nosenko and J. Goree, *Phys. Rev. Lett.* **93**, 155004 (2004).
- [54] Y. Feng, J. Goree, and B. Liu, *Phys. Rev. Lett.* **109**, 185002 (2012); *Phys. Rev. E* **86**, 056403 (2012).
- [55] D. Huang, S. Lu, and Y. Feng, *Phys. Rev. E* **103**, 013211 (2021).
- [56] C. K. Birdsall and A. B. Langdon, *Plasma Physics via Computer Simulation* (Institute of Physics Publishing, Bristol, 1991).
- [57] T. E. Sheridan, V. Nosenko, and J. Goree, *Phys. Plasma* **15**, 073703 (2008).
- [58] T. Egami, K. Maeda, and V. Vitek, *Philos. Mag. A* **41**, 883 (1980).
- [59] H. Rafii-Tabar, *Phys. Rep.* **390**, 235 (2004).